Finite Control Set Model Predictive Control With Floating Virtual Voltage Vectors for Grid-Connected Voltage Source Converter

Piotr Falkowski, Andrzej Sikorski, and Mariusz Malinowski, *Fellow, IEEE*

***Abstract*—This article presents a new algorithm of finite control set model predictive control (FCS-MPC) with floating virtual voltage vectors (VVs) applied to grid-connected voltage source converter. The new solution improves the conventional FCS-MPC and FCS-MPC with virtual VVs, assuring a fixed switching frequency. In comparison with FCS-MPC using virtual VVs, the proposed algorithm ensures a shorter distance between floating virtual VVs and actual voltage vector achieves lower THDi and ripples of the grid current for the same sampling time. The proposed control method has been experimentally validated using a 5-kW prototype. The algorithm was examined and compared in steady and transient states as well as under grid voltage disturbances, such as higher harmonics, dips, and unbalance. The simulation results and experimental measurements confirm that the developed control technique shows a high quality of the grid current (low THDi value), high dynamic performance, and immunity in case of weak grid conditions.**

***Index Terms*—AC–DC power conversion, current control, harmonic distortion, predictive control.**

I. Introduction

GRID connected ac–dc voltage source converters (VSC) because of their advantages, such as sinusoidal grid current, bidirectional power flow, smaller ripple of the dc link voltage are becoming more and more popular in industry [1], [2]. In these converters grid current vector components or directly, active and reactive power are controlled by various conventional methods well known from literature [3]—[5]. In all cases, the indirect or direct effect of control are sinusoidal grid currents with low THDi (low current ripples). However, conventional methods were usually designed for the ideal grid and they are sensitive to grid voltage disturbances, such as higher harmonics, dips, and unbalance [4].

Besides of abovementioned conventional control methods recently is also popular deadbeat (DB) control, which is characterized by theoretically high dynamic during transients and good steady-state characteristics. Unfortunately, the main disadvantages of DB control is low resistance to parameter mismatch (e.g., inductance in grid-connected VSC), unmodeled delays and other errors in the model, what was described in [6]–[8]. The main reason for these inconveniences is the indirect control of the grid current by determining a reference converter voltage and its reproduction by space vector modulator (SVM). Without the modulation process and switching actions taken into account, dead-time errors, uncompensated delays, and inductance model errors are accumulated [6]–[8]. Another disadvantage of DB control is that nonlinearities and constraints of the system variables are difficult to implement in industry [8].

Therefore, another well-established concept, model predictive control (MPC) appears interesting alternative for grid connected VSC. Especially, MPC methods with finite control set (FCS-MPC) and continuous control set (CSS-MPC) have become competitive compared to traditional control methods due to their robustness under the grid voltage disturbances, parameters uncertainty, or high dynamic performances [9]–[12].

Currently, FCS-MPC is one of the fastest developing MPC control strategies [13], [14]. In contrast to linear controllers with pulse width modulation (PWM), FCS-MPC uses the discrete nature of power converters. It employs all the possible output voltage vectors (VVs) of the converter as a control set to perform the prediction and the optimization of the cost function and to select appropriate output voltage vector. The FCS-MPC is characterized by the following:

1) the possible inclusion of constraints;
2) simple implementation;
3) a fast dynamic response;
4) easy application in a multiobjective system as a result of the flexible design of the cost function.

Thanks to its advantages, the FCS-MPC approach has been used in various power electronic applications, e.g., active power filters [15], current source converters [16], [17], multilevel converters [18], matrix converter [19], and dc–dc converter [20]. It

Manuscript received October 30, 2020; revised January 14, 2021; accepted March 14, 2021. Date of publication March 19, 2021; date of current version June 30, 2021. This work was supported in part by the scientific subsidy of the Ministry of Science and Higher Education under Grant WZ/WE-IA/5/2020 and in part by the TEAM-TECH/2016-1/5 Project carried out within the TEAM-TECH program of the Foundation for Polish Science cofinanced by the European Union under the European Regional Development Fund. Recommended for publication by Associate Editor T. Dragicevic. *(Corresponding author: Piotr Falkowski.)*

Piotr Falkowski and Andrzej Sikorski are with the Faculty of Electrical Engineering, Bialystok University of Technology, 15-351 Bialystok, Poland (e-mail: p.falkowski@pb.edu.pl; a.sikorski@pb.edu.pl).

Mariusz Malinowski is with the Department of Electrical Engineering, Warsaw University of Technology, 00-661 Warsaw, Poland (e-mail: malin@isep.pw.edu.pl).

Color versions of one or more figures in this article are available at https://doi.org/10.1109/TPEL.2021.3067602.

Digital Object Identifier 10.1109/TPEL.2021.3067602

is possible to use weighting factors also to change or limit the value of average switching frequency [21], [22], or to control common-mode voltage [23]. Hard constraints were used in predictive control of the speed of induction motors [24]. In spite of its advantages, this control strategy has some open problems, which have to be resolved as follows:

1) the necessity to select weighting factors;
2) variable switching frequency;
3) only one voltage vector applied during the switching period.

To resolve the first problem, i.e., weighting factor selection, an algebraic criterion for predictive torque and flux control has been proposed in [25]. A sequential model predictive control with separate cost functions for torque and flux [26] and parallel predictive torque control [27] were proposed to avoid weighting factors and overcome the difficulties of their selection. Moreover, in [28], the torque and flux error-based cost function of conventional model predictive torque control was replaced by the voltage vector tracking error-based cost function.

The second and the third problem, i.e., the variable switching frequency and the fact that a single voltage vector is utilized for the entire sampling time is particularly unwanted in a grid-connected VSC. This kind of converter, to meet the grid code requirements, should ensure high quality of the grid current (low value of THDi). Therefore, the grid current ripple should be minimized without increasing the value of filter inductance, cost and dimensions of the converter. In order to obtain this in conventional FCS-MPC, the sampling time should be as short as possible. This can require the use of more powerful (and therefore more expensive) DSPs or FPGAs, which may be not acceptable for low cost industrial applications. Moreover, increase of sampling frequency does not solve the problem of variable switching frequency (difficulties with choosing appropriate EMI filters still persists).

Several strategies have been proposed to eliminate these disadvantages. In [29], VVs selected by means of the FCS-MPC algorithm are filtered out using the low-pass filter extracting the low-frequency component (the reference voltage vector) and next the reference voltage vector is modulated through a sinusoidal PWM. Nevertheless, this methodology slows down the dynamic response.

Another control strategy is modulated MPC (M^2PC), which allows us to obtain fixed switching frequency using a SVM and preserving the desired characteristics of FCS-MPC [30], [31]. However, the drawback of this technique is high computational effort and slightly worse performance using a multiobjective cost function [31].

Another solution to the abovementioned problems was the use of virtual VVs [32]–[35], which are reproduced using digital SVM (DSVM). This method can be used in a 2-level VSC and change it in terms of its properties into a multilevel converter. The control idea of using virtual VVs basically does not limit the number of vectors that can be created. In this way, we can achieve partially fixed switching frequency and reduce the grid current ripple (lower THDi). Generally, the more virtual VVs means the smaller area of triangles created by the virtual VVs and in consequence the lower THDi value. Nevertheless, this dramatically increases the computational burden during the selection of the best VV by calculating the cost function.

The next step was the use of preselection methods to narrow down the number of considered virtual VVs that in consequence cause reduction of the calculation time [33]–[38]. However, these interesting solutions require an additional algorithm to operate in a dynamic state [33] and they are designed for the DSVM with 38 VVs (virtual and basic) [33]–[35]. Methods [37], [38] are characterized by sensitivity to the inductance changes as well as a lack of a clear manner how to choose the number of analyzed virtual vectors.

The purpose of this article is to solve the abovementioned issues by proposed method with floating virtual VVs. Those vectors are computed online in a short distance from the reference voltage vector, which should be realized by the converter to obtain the reference grid current. All VVs (reference and floating virtual VVs) are reproduced through SVM using three basic VVs. The closer floating virtual VVs to the reference voltage vector means the smaller grid current ripples. This method, thanks to SVM, allows us to obtain a fixed switching frequency and low THDi of the grid current without decreasing of the sampling period. Furthermore, simulation and experimental tests have shown that the proposed method is characterized by high robustness to grid voltage disturbances and parameter mismatch.

This article is organised as follows. In Section II, a predictive model of the system was overviewed and description of the conventional FCS-MPC is shown in Section III. The FCS-MPC with virtual VVs was discussed in Section IV and the proposed new FCS-MPC with floating virtual VVs was presented in Section V. The impact of the inductance *L* changes was explained in Section VI. Simulation and experimental results were shown in Section VI. Finally, Section VII concludes this article.

II. System Overview

Fig. 1(a) shows a two-level ac–dc voltage source converter connected to the grid using a passive L filter. This system can be described by the following relationship in a stationary $\alpha\beta$ frame (assuming that resistance of the filter ≈ 0):

$$\boldsymbol{e}_{\alpha\beta} = L\frac{d}{dt}\boldsymbol{i}_{\alpha\beta} + \boldsymbol{u}_{\alpha\beta}. \tag{1}$$

Using the Park transformation, (1) can be described in a *dq* rotating reference frame

$$\boldsymbol{e}_{dq} = L\frac{d}{dt}\boldsymbol{i}_{dq} + j\omega_g L\boldsymbol{i}_{dq} + \boldsymbol{u}_{dq} \tag{2}$$

where

$\boldsymbol{e}_{dq}$ grid voltage vector in the *dq* rotating reference frame;
$\boldsymbol{i}_{dq}$ grid current vector in the *dq* rotating reference frame;
L inductance of the L filter;
ω_g grid pulsation.

The converter basic VVs in the *dq* rotating reference frame can be defined as

$$\boldsymbol{u}_{dq} = \begin{cases} \frac{2}{3}U_{\mathrm{dc}}e^{j[(n-1)\frac{\pi}{3}-\omega_{\mathrm{g}}t]} : \text{for}\, n = \{1,2,3,4,5,6\} \\ \qquad\qquad\qquad\qquad\quad ''0'' : \text{for}\, n = \{0,7\}. \end{cases} \tag{3}$$

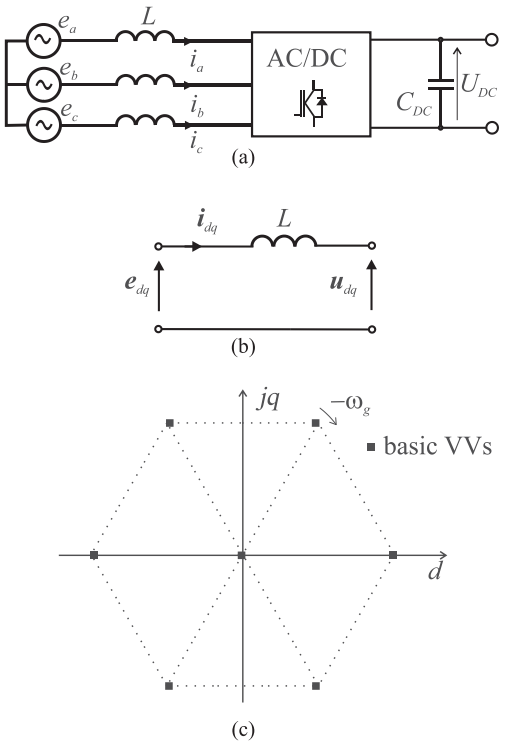

Fig. 1. (a) Schematic diagram of two-level VSC. (b) Equivalent circuit of VSC with L filter. (c) Basic VVs of a two-level VSC.

Fig. 1(c) shows a graphical representation of converter's basic VVs in the *dq* rotating reference frame. It should be noted that the basic VVs rotate in the coordinate system *dq* with pulsation ω_g in a clockwise direction. An equivalent circuit diagram described by the relationship (2) is presented in Fig. 1(b). Such a topology allows making use of eight possible switching states, leading to seven basic VVs at the input of the converter. Based on (2) for further considerations, the actual voltage vector $\boldsymbol{u}_{1h}$ can be defined as follows [5]:

$$\boldsymbol{u}_{1h} = \boldsymbol{e}_{dq} - j\omega_g L \boldsymbol{i}_{dq}. \tag{4}$$

Taking into account (4) and (2), the following can be introduced:

$$L\frac{d}{dt}\boldsymbol{i}_{dq} = \boldsymbol{u}_{1h} - \boldsymbol{u}_{dq}. \tag{5}$$

Equation (5) will be used to predict the location of the current vector in the next sampling step using control in microprocessor.

III. FCS-MPC Using a Single Voltage Vector

FCS-MPC method uses the discrete nature of power converters characterized by a limited number of converter basic VVs to predict the future action of the controlled variables. Calculations are performed in each sampling step for all switching states. The selection of an optimal converter basic voltage vector is made by minimizing the defined cost function *J*. One of the main advantages is multivariable control of various physical variables in a single cost function. Another valuable feature

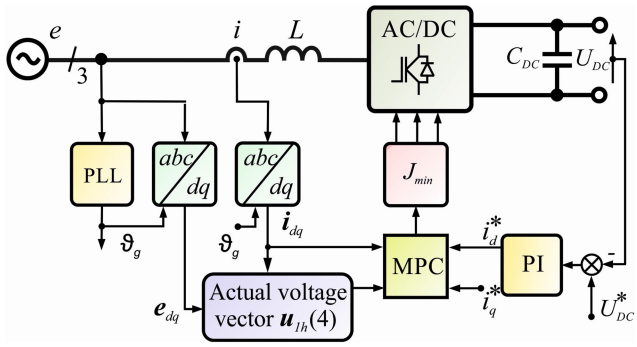

Fig. 2. Block diagram of conventional FCS-MPC.

is the possibility of introducing desired constrains or parameter optimization criteria in the cost function. The schematic diagram of conventional FCS-MPC has been shown in Fig. 2. The main control objective of ac–dc converters is tracking their references, i.e., the grid current vector components i_d^* and i_q^* that are proportional to active and reactive power, respectively. The measuring of the actual values of currents and voltages (step k) starts the prediction process. The derivative of the grid current vector is approximated using the forward Euler discretization method with sampling time T_s

$$\frac{d}{dt}\boldsymbol{i}_{dq} \approx \frac{\Delta \boldsymbol{i}_{dq}(k+1)}{T_s} = \frac{\boldsymbol{i}_{dq}(k+1) - \boldsymbol{i}_{dq}(k)}{T_s}. \tag{6}$$

Using (5) and considering (6) the future grid current vector $\boldsymbol{i}_{dq}(k+1)$ is predicted

$$\Delta \boldsymbol{i}_{dq}(k+1) = \frac{\boldsymbol{u}_{1h}(k) - \boldsymbol{u}_{dq}(k)}{L} T_s \tag{7}$$

$$\boldsymbol{i}_{dq}(k+1) = \boldsymbol{i}_{dq}(k) + \Delta \boldsymbol{i}_{dq}(k+1). \tag{8}$$

It can be assumed that for sufficiently small sampling time T_s, the reference grid current vector $\boldsymbol{i}_{dq}^*(k)$ does not change

$$\boldsymbol{i}_{dq}^*(k+1) \approx \boldsymbol{i}_{dq}^*(k). \tag{9}$$

Next, using the predicted value of the grid current (8) and the reference current (9), the future error of grid current vector is determined

$$\boldsymbol{\varepsilon}_{idq}(k+1) = \boldsymbol{i}_{dq}^*(k+1) - \boldsymbol{i}_{dq}(k+1). \tag{10}$$

The optimal converter basic voltage vector $\boldsymbol{u}_{dq}(k)$, which will be applied during the next sampling time T_s is chosen by calculating the cost function *J* (11). The switching combination $\boldsymbol{u}_{dq}(k)$, which gives the minimum value of the cost function *J* (11) will be chosen. The primary objective of the presented cost function *J* (11) is to minimize the error between the references $\boldsymbol{i}_{dq}^*(k+1)$ and the future predicted grid current vector $\boldsymbol{i}_{dq}(k+1)$ obtained through the prediction process

$$J = \varepsilon_{id}^2(k+1) + \varepsilon_{iq}^2(k+1). \tag{11}$$

The nature of the operation of the microprocessor control system causes a delay between the start of sampling and the selection of a new converter basic voltage vector (sending new switching state). This delay is caused, among other things, by

a specific conversion time of the analogue to digital converter and the calculation time. This issue was solved with a simple delay compensation scheme using the same equations but with the shift one step forward in time [39].

IV. FCS-MPC With Virtual VVs

With the development of power semiconductors, the maximum possible switching frequency of converters increases. Thanks to this, it is possible, e.g., to decrease the THDi of grid current (increase the quality) or maintain the same THDi and reduce filter inductance and as a consequence reduce the dimensions and cost of the converter. In the conventional FCS-MPC, in which the single voltage vector is utilized for the whole sampling time, the switching frequency f_{sw} depends on the sampling time T_s and it cannot be higher than $f_{sw} \leq (1/2 \cdot 1/T_s)$ [32]. In practice, the average switching frequency $f_{\mathrm{sw}\,(av)}$ of the ac–dc grid converter is a few times smaller than $1/T_s$. Therefore, to achieve a higher average switching frequency and use the advantages of wide-bandgap semiconductors the sampling time should be as short as possible. To obtain that, it is necessary to use very fast and more expensive DSPs or FPGAs, which is a huge disadvantage in the context of industrial implementation. Some improvements, which in various ways try to solve this issue, were presented in Section I. One of them is the virtual VVs concept obtained by the DSVM technique.

The idea of virtual VVs is to increase the available VVs while maintaining a discrete description of the operation of the converter. Virtual VVs are generated by the combination of two or three switching states during a single sampling interval. In other words, virtual VVs are formed by a linear combination of basic VVs, where each basic voltage vector is used in a switching sequence for a certain time [32]. To reproduce virtual VVs, SVM (called DSVM because of the use of a discrete map of switching combinations) is used.

The number of virtual VVs is connected with the number of subdivisions of the sampling period. With the increase in the number of divisions, the total number of virtual VVs also grows to ensure better performance. However, the calculation burden during the selection of the best switching combination by the evaluation of the cost function J grows dramatically. For example, if in a 2-level ac–dc converter the number of subdivisions of the sampling period is 2, the whole number of VVs is 20 (8 basic and 12 virtual), like in a 3-level converter. When the number of subdivisions is 3, the total number of VVs is 38 (8 basic and 30 virtual) (see Fig. 3). In order to record virtual VVs in the look-up table in the further part of this article, the name fixed virtual VVs will be also used. The control algorithm of FCS-MPC with fixed virtual VVs is almost the same as in the conventional FCS-MPC described previously. The main differences are as follows:

1) (depending on the number of subdivisions) 20 or 38 VVs are analyzed instead of 8 VVs;
2) it is necessary to use a modulator to reproduce the virtual VVs.

One of the main advantages of FCS-MPC with virtual VVs is that the control algorithm may operate with longer sampling time achieving lower current ripples compared to conventional FCS-MPC using single voltage vector during the same sampling period. Moreover DSVM leads to a partially constant switching frequency of the transistors, which can help with the design of passive filters. However, the higher number of analyzed VVs during each sampling period cause to the longer computation time. Therefore, a need for a wise way to preselect virtual switching states in each sampling time arises. Some ideas that allow reducing the number of VVs analyzed in each control step have already been proposed in [33]–[35]. Nevertheless, the mentioned algorithms are designed to divide the sampling period into three subdivisions. Therefore, more divisions of the sampling time, with the aim of improving the performance, could render the proposed techniques of preselection useless. Furthermore, dividing the sampling time in three or even four subdivisions does not guarantee that the distance from the actual voltage vector $\boldsymbol{u}_{1h}$ to the three nearest virtual VVs is minimal (and thus the lowest current ripples are achieved).

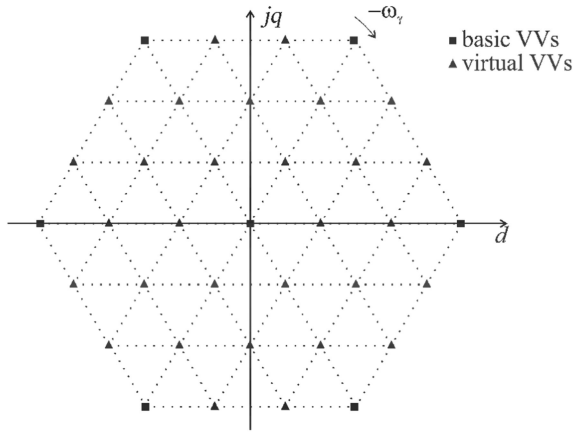

Fig. 3. Voltage vectors (8 basic and 30 virtual) for the number of the subdivision – 3.

V. FCS-MPC With Floating Virtual VVs

To overcome the abovementioned drawbacks, this article proposes a solution, which ensures higher performance without a significant increase of computational time. The main idea of the method is to use floating virtual VVs computed online basing on the reference voltage vector instead of using fixed virtual VVs given in the look-up table. In the discussed method, we distinguish three categories/levels of VVs: basic VVs, a reference voltage vector $\boldsymbol{u}^*_{dq}$ and floating virtual VVs. A graphic interpretation of the above mentioned VVs is presented in Fig. 4. The reference voltage $\boldsymbol{u}^*_{dq}$ is most often used in a steady state, which makes the method similar to the DB-SVM method [6]–[8]. The second voltage level is the vectors located at the vertices of the triangle inscribed in the circle with a radius of R, the so-called floating virtual VVs (FVVVs). FVVVs are used to correct control errors caused by inaccuracies in determining the parameters of the real system, including the inductance L. The third voltage level are basic VVs (six active and two zero). These VVs are used when there are significant deviations of the system

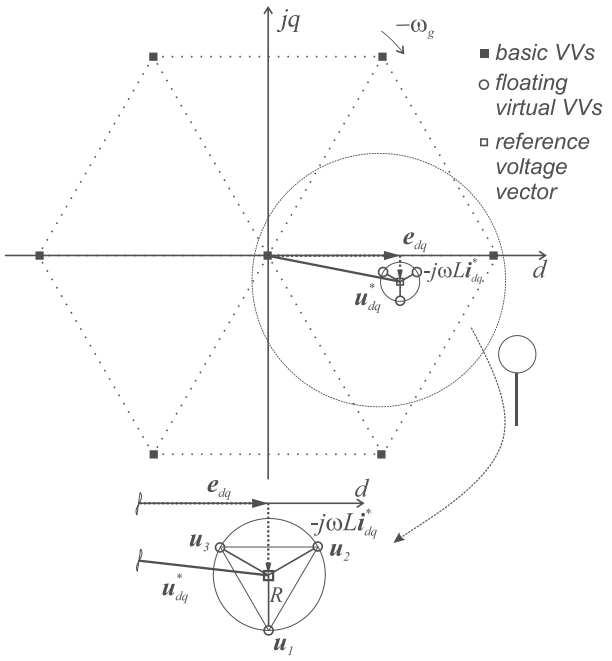

Fig. 4. Illustration of the reference voltage vector (13), floating virtual VVs (14)–(16) and basic VVs (3).

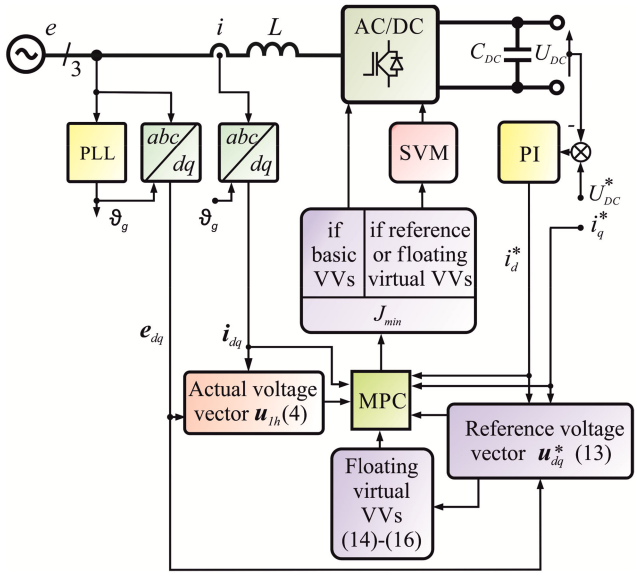

Fig. 5. Block diagram of the proposed FCS-MPC with floating virtual VVs.

parameters from the real values, e.g., L from L_m, and especially during dynamic states with large step changes of the reference current value.

The reference voltage vector $\boldsymbol{u}^*_{dq}$ is determined using the reference grid current vector i^*_{dq} in the following equation:

$$\boldsymbol{u}^*_{dq} = \boldsymbol{e}_{dq} - j\omega_g L \boldsymbol{i}^*_{dq}. \tag{12}$$

The voltage vector u^*_{dq} determines the reference voltage, which should be reproduced by the converter to obtain the reference current vector $\boldsymbol{i}^*_{dq}$. However, due to errors, e.g., in measurements, parameters of the model, etc., using only the reference voltage vector $\boldsymbol{u}^*_{dq}$ does not allow to achieve the controllability of the converter. Due to this, the next idea is to use three floating virtual VVs to compensate undesirable errors. Those floating virtual VVs are created basing on the reference voltage vector $\boldsymbol{u}^*_{dq}$. The floating virtual VVs are described as vertices of an equilateral triangle whose center is the reference voltage vector $\boldsymbol{u}^*_{dq}$. In this way, the created floating virtual VVs ensure minimal deviations of the current from the reference value (reduce its ripple and harmonics). The floating virtual VVs cannot be too close to the reference voltage vector $\boldsymbol{u}^*_{dq}$. Due to the model errors the actual voltage vector $\boldsymbol{u}_{1h}$ (4) could be outside the area determined by floating virtual VVs, which will result in higher current ripple. This problem was clearly described in Section VI. The reference voltage vector $\boldsymbol{u}^*_{dq}$ and floating virtual VVs are analyzed together with basic VVs by the control algorithm as one of the possible voltages, which will be reproduced by the converter. Detailed descriptions are given in the following discussion.

The block diagram of the FCS-MPC with floating virtual VVs is shown in Fig. 5. As it was already mentioned, the main control objective of ac–dc converters is tracking their references, i.e., the grid current vector components i^*_d and i^*_q that are proportional to active and reactive power, respectively. The proposed control algorithm also uses assumptions (6) and (9). The algorithm is described in dq rotating reference frame oriented on the grid voltage vector $\boldsymbol{e}_{dq}$. The reference grid current component i^*_d is a product of a dc-link voltage controller, i^*_q is proportional to reactive power Q^*, both are used to compute the reference voltage vector $\boldsymbol{u}^*_{dq}(k)$

$$\boldsymbol{u}^*_{dq}(k) = \boldsymbol{e}_{dq}(k) - j\omega_g L \boldsymbol{i}^*_{dq}(k). \tag{13}$$

Basing on the reference voltage vector $\boldsymbol{u}^*_{dq}(k)$, the three-floating virtual VVs $\boldsymbol{u}_1(k)$, $\boldsymbol{u}_2(k)$, $\boldsymbol{u}_3(k)$ are obtained

$$\boldsymbol{u}_1(k) = \boldsymbol{u}^*_{dq}(k) - jR \tag{14}$$

$$\boldsymbol{u}_2(k) = \boldsymbol{u}^*_{dq}(k) + R\frac{\sqrt{3}}{2} + j\frac{1}{2}R \tag{15}$$

$$\boldsymbol{u}_3(k) = \boldsymbol{u}^*_{dq}(k) - R\frac{\sqrt{3}}{2} + j\frac{1}{2}R \tag{16}$$

where R is the maximal distance of the three floating virtual VVs from the reference voltage vector $\boldsymbol{u}^*_{dq}(k)$. These three vectors should form an equilateral triangle inscribed in a circle with the radius R (see Fig. 4).

Equation (17) is used to predict the change of the grid current vector in the sampling time for converter VVs $\boldsymbol{u}_{\mathrm{conv}}(k)$. When calculating the predicted change of the grid current vector (17), $\boldsymbol{u}_{\mathrm{conv}}(k)$ is substituted with: one reference voltage vector $\boldsymbol{u}^*_{dq}(k)$ described using (13), three floating virtual VVs $\boldsymbol{u}_1(k)$, $\boldsymbol{u}_2(k)$, $\boldsymbol{u}_3(k)$ defined using (14)–(16), and seven basic VVs described using (3)

$$\Delta \boldsymbol{i}_{dq}(k+1) = \frac{\boldsymbol{u}_{1h}(k) - \boldsymbol{u}_{\mathrm{conv}}(k)}{L} T_s. \tag{17}$$

Theoretically, only one reference voltage vector and three floating virtual VVs need to be analyzed, however, to ensure better operation in dynamic states seven basic VVs are also considered. This shortens the duration of transient states. Using (17), the future grid current vector $\boldsymbol{i}_{dq}(k+1)$ is predicted

$$\boldsymbol{i}_{dq}(k+1) = \boldsymbol{i}_{dq}(k) + \Delta\boldsymbol{i}_{dq}(k+1). \tag{18}$$

Next, using the predicted value of the grid current (18) and the reference current, the future error of grid current vector is determined

$$\boldsymbol{\varepsilon}_{idq}(k+1) = \boldsymbol{i}^{*}_{dq}(k+1) - \boldsymbol{i}_{dq}(k+1). \tag{19}$$

Like in the conventional FCS-MPC the algorithm uses the cost function J to select the optimal converter voltage vector $\boldsymbol{u}_{\mathrm{conv}}(k)$ and a simple delay compensation scheme, similar to one proposed in [39]. However, in the proposed method the algorithm evaluates J for one reference voltage vector, three floating virtual VVs, and seven basic VVs

$$J = \varepsilon^{2}_{id}(k+1) + \varepsilon^{2}_{iq}(k+1). \tag{20}$$

VI. Impact of the Inductance L Changes

Changes or incorrect determination of the total inductance L between the voltage source and the converter cause errors in reconstructing of the reference grid current vector $\boldsymbol{i}^{*}_{dq}$. That is why it is so important to analyze the impact of inductance changes on the operation of the converter controlled by all algorithms. In this article, the changes in the inductance L were carried out by changing the modeled inductance L_m used in the control algorithm.

In the proposed control method with floating virtual VVs, an error may also occur when determining the reference voltage $\boldsymbol{u}^{*}_{dq}$ (12). The error in determining the inductance L causes a change in the voltage vector component $-j\omega_g L\boldsymbol{i}^{*}_{dq}$ in the $\boldsymbol{u}^{*}_{dq}$ vector, and consequently a change in the position of the triangle defining the floating virtual VVs $\boldsymbol{u}_1$, $\boldsymbol{u}_2$, $\boldsymbol{u}_3$ (see Fig. 6). If $L = L_{\mathrm{m}}$ [see Fig. 6(a)], the $\boldsymbol{u}_{1h}$ voltage vector is located inside the triangle. In this case, vectors proportional to current derivative specified by (5) and the predicted changes of the grid current (17) allow the current vector $\boldsymbol{i}_{dq}$ to be controlled.

Fig. 6(d) presents a situation in which the actual voltage vector $\boldsymbol{u}_{1h}$ is outside the triangle defining the considered floating virtual VVs. In this case, as indicated by vectors proportional to the current derivative presenting the predicted changes of the grid current [see Fig. 6(d)], every voltage vector increases the current module so that full control over current regulation is lost. What distinguishes the proposed method from others is the way of operation, when the actual voltage vector $\boldsymbol{u}_{1h}$ goes beyond the triangle created by the floating virtual VVs. In this case, basic vectors are used that prevent loss of control over the controlled current.

The correct operation of the proposed algorithm is determined by the appropriate value of radius R defining the floating virtual VVs triangle. As a rule, this triangle should be as small as possible (this results in maximum limitation of higher harmonics). On the other hand, R decides when we lose control over the current

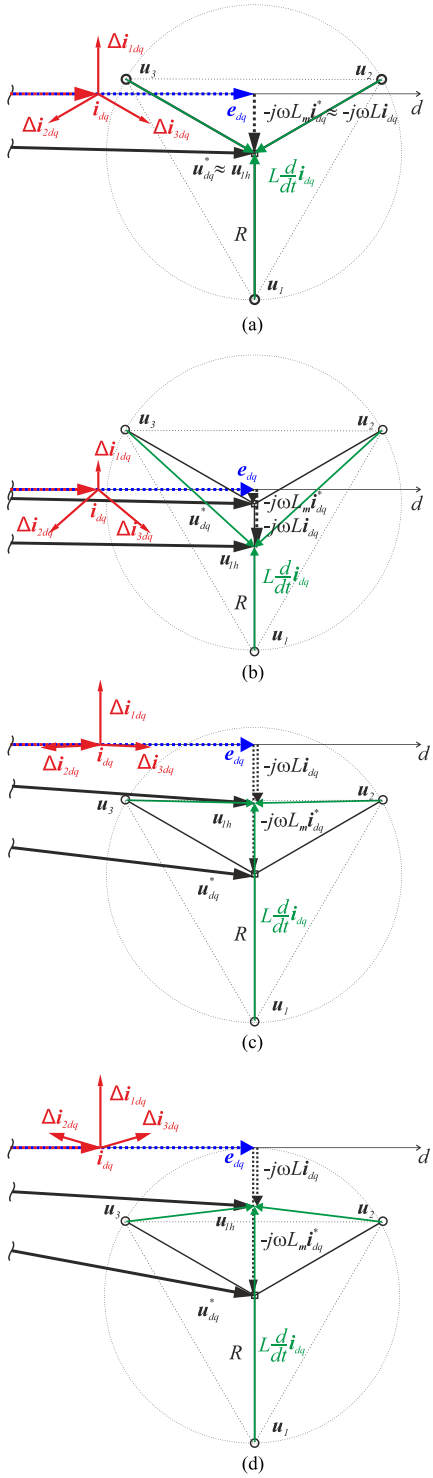

Fig. 6. Illustration presenting influence of the L/L_m change for current regulation. (a) $L/L_m = 1$. (b) $L/L_m = 4$. (c) $L/L_m = 0.44$. (d) $L/L_m = 0.4$.

caused by a change of the inductance L in relation to the value of the model inductance L_m [see Fig. 6(c)]. The radius R affects the lengths of the vectors $L\boldsymbol{di}_{dq}/dt$ (see Fig. 6) connecting the vertices of the triangle inscribed in the circle, with the radius R, with the tip of the voltage vector $\boldsymbol{u}_{1h}$ (corresponding to the

TABLE I
SYSTEM PARAMETERS

Variable	Parameters	Value
e	Grid-voltage	230 Vrms
U_{DC}	DC-link voltage	650 V
T_s (f_s)	Sampling time (sampling frequency)	50 µs (20 kHz)
L	Filter inductance	5.2 mH
C_{DC}	DC-link capacitance	1.1 mF
ω_g	Grid pulsation	314 rad/s
R	Maximal distance of three floating virtual VVs from the reference voltage vector	25 V

voltage forcing the grid current). In a boundary situation [see Fig. 6(c)], the difference of the voltage vectors is equal to half the radius R

$$\omega_g L_m \boldsymbol{i}^*_{dq} - \omega_g L \boldsymbol{i}_{dq} = 0.5R. \tag{21}$$

Assuming that $\boldsymbol{i}_{dq} \approx \boldsymbol{i}^*_{dq}$, the minimum radius of the circle is

$$R = 2\omega_g \Delta L \left|\boldsymbol{i}^*_{dq\_\max}\right| \tag{22}$$

where

$|\boldsymbol{i}^*_{dq\_\max}|$ module of the maximum reference value of the grid current vector;

$\Delta L = |L_m\text{-}L|$ maximum expected inductance change.

The radius R is determined at the beginning of control operation and is permanently stored as parameter of the control algorithm.

VII. SIMULATION AND EXPERIMENTAL STUDIES

A. Simulations Studies

Simulation studies were performed on a two-level VSC. The parameters of the system have been shown in Table I. Simulations were carried out in MATLAB/Simulink software. Comparative tests were performed for the proposed FCS-MPC with floating virtual VVs and two other methods described in this article, i.e., conventional FCS-MPC, and FCS-MPC with fixed virtual VVs. Additionally, tests were performed for the methods which use the deadbeat principles, i.e., conventional deadbeat with SVM modulator (DB-SVM) [6]–[8] and DB-FCS-MPC with fixed virtual VVs [35], [38].

The simulated waveforms of the phase grid voltage ea and current ia for the compared methods were shown in Fig. 7 (for L = Lm). The presented results in a steady state were obtained for active power P = 3 kW, and reactive power Q = 0 Var. As it was shown in Fig. 7 and Table II, the FCS-MPC with floating virtual VVs (the proposed method) gives almost the same THDi of the grid current as the conventional DB-SVM as well as has constant switching frequency at 20 kHz [see

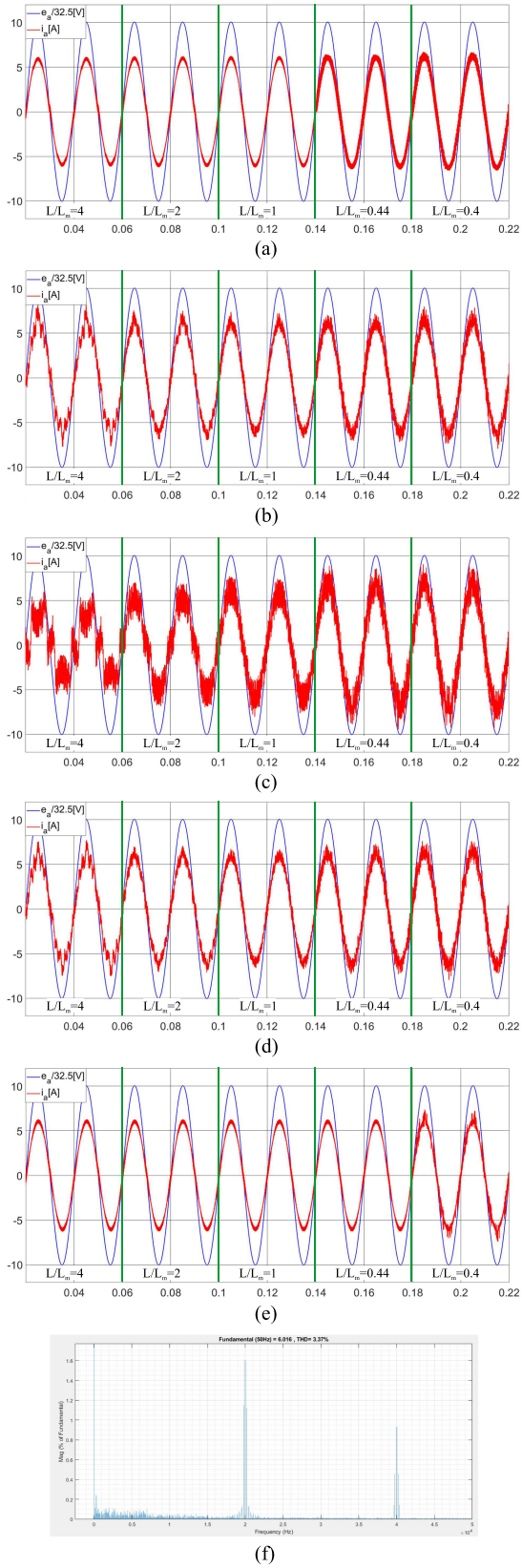

Fig. 7. Grid phase voltage e_a and current i_a for different L/L_M ratios for five control strategies: (a) DB-SVM, (b) DB-FCS-MPC with fixed virtual VVs, (c) FCS-MPC, (d) FCS-MPC with fixed virtual VVs, (e) FCS-MPC with floating virtual VVs. (f) Frequency spectrum of the grid current i_a for FCS-MPC with floating virtual VVs – THDi = 3.4%.

TABLE II
THDI [%] VALUES FOR DIFFERENT L/L_M RATIOS

Method	$L/L_M=4$	$L/L_M=2$	$L/L_M=1$	$L/L_M=$ 0.44	$L/L_M=$ 0.4
DB-SVM	4.16	3.64	3.32	10.4	10.6
DB-FCS-MPC with fixed virtual VVs	14.3	9.4	7.67	11.2	12.7
FCS-MPC	62.2	26.8	20.9	19.0	19.3
FCS-MPC with fixed virtual VVs	13.2	8.68	7.3	10.3	12.3
FCS-MPC with floating virtual VVs	3.35	3.35	3.37	3.44	8.18

Fig. 7(f)]. The current is sinusoidal with low ripples and, as it was proven the proposed method gives very good results in a steady state compared to other examined algorithms from the FCS-MPC family.

An important feature of the predictive methods is the dependence of their accuracy on matching the parameters of the model to the actual system. Simulation tests of the change in the inductance L, were carried out by changing the modeled inductance Lm used in the control algorithm, what affected the L/L_m ratio, are shown in Table II and Fig. 7.

The most robust was the proposed control method FCS-MPC with floating virtual VVs. The variation of L/L_m from 0.44 to 4 caused that L_m value was in range from 11.8 mH to 1.3 mH and it practically did not influence the value of the THDi current [see Fig. 7(e) and Table II]. In Fig. 6(b) and (c), the tip of the voltage vector $\boldsymbol{u}_{1h}$ does not leave the area of the defined triangle. As a result, directions of the predicted current vector changes allow to preserve the control of the current $\boldsymbol{i}_{dq}$. The reduction of L/L_m from 1 to 0.4 results in current deformations (THDi increase to 8.18%). In this case, the voltage vector $\boldsymbol{u}_{1h}$ is outside the floating virtual VVs triangle ($L/L_m = 0.4$) and the predicted changes of the current do not allow to control the grid current (all directed upwards) [see Fig. 6(d)]. In this case, basic VVs, which prevent the loss of control over the controlled current are used. A conventional FCS-MPC algorithm reacts particularly badly to the increase in L/L_m to 4, where there is a clear reduction in the amplitude of the reproduced current [see Fig. 7(c)]. Subsequent methods, i.e., FCS-MPC with fixed virtual VVs and DB-FCS-MPC with fixed virtual VVs are characterized by similar sensitivity to the change in the inductance L_m [see Fig. 7(b) and (d)]. In the case of the DB-SVM method, when $L/L_m>1$, the THDi value increases slightly [see Fig. 7(a)]. This method is much more sensitive when $L/L_m<1$. In this case, there is a significant increase in the THDi of the grid current (see Table II).

Three cases were shown in Fig. 8 during step changes of the reference grid current i_d^* from 6 A to –6 A (inverter mode) and back to 6 A (3 kW). In the first case [see Fig. 8(a)], the conventional FCS-MPC method with a very fast dynamic

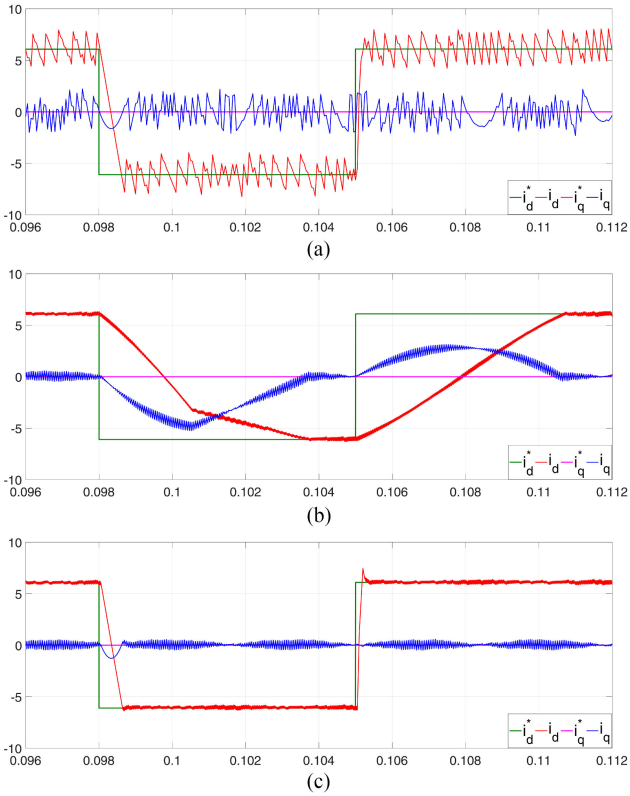

Fig. 8. Step changes of reference grid current component i_d^* for: (a) conventional FCS-MPC with 7 basic VVs, (b) proposed FCS-MPC with only 4 VVs (1 reference and 3 floating virtual VVs), (c) proposed FCS-MPC with 11 VVs (1 reference, 3 floating virtual, and 7 basic VVs).

response was examined for better comparison. In the second case [see Fig. 8b)], the control algorithm operating only with 4 VVs (without basic VVs) was taken into account and in the last case [see Fig. 8(c)], the proposed algorithm used 11 VVs (one reference voltage vector, three floating virtual VVs, and seven basic VVs), as presented in Section V. It can be noticed that the removal of the basic VVs from the proposed algorithm drastically deteriorates the dynamic response [see Fig. 8(b)]. That is because the algorithm uses only 4 VVs, which are very close to the actual voltage vector $\boldsymbol{u}_{1h}$ and the corresponding derivatives (components responsible for the current change) are short. This situation is very desirable in a steady state because it guarantees the lowest current ripple, however, it has a negative impact on the duration of transient states. Therefore, an appropriate basic voltage vector is also needed because it gives a long derivative, which shortens the transition time [see Fig. 8(c)]. Thanks to this the proposed method has the same, i.e., very fast dynamic performance as the conventional FCS-MPC [see Fig. 8(a)].

B. *Experimental Studies*

To experimentally validate the proposed control strategy 2-level IGBT-VSC was built and low-cost microcontroller STM32F7 based on an ARM Cortex-M7 core was implemented as control platform. The computational burden for the microcontroller was very low for all control methods presented in the paper because the calculation time for the proposed method was

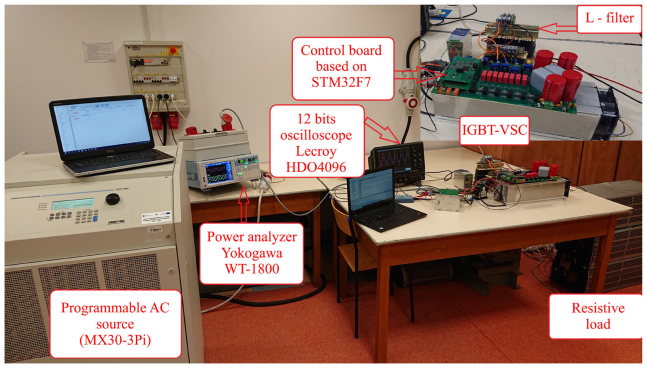

Fig. 9. Experimental setup.

TABLE III
COMPARISON OF THDi FACTORS IN THE STEADY STATE

Control method	THDi [%]
FCS-MPC with fixed virtual VVs	5.9
FCS-MPC with floating virtual VVs (proposed method)	2.3

12.9 μs (25.8% of computational burden) while for the conventional FCS-MPC it was 10.8 μs (21.6% of computational burden) and for the FCS-MPC with fixed virtual VVs it was 17.4 μs (36.8% of computational burden). All parameters were exactly as in the simulations (see Table I). A programmable ac source (MX30-3Pi) was used to power the VSC. The measurement of the THD factor was made using the power analyzer Yokogawa WT-1800. The experimental setup was shown in Fig. 9.

This section validates the feasibility of the proposed control technique by experiments. First, two algorithms: the FCS-MPC with fixed virtual VVs and the proposed FCS-MPC with floating virtual VVs, have been compared in a steady state [see Fig. 10]. The dc-link of VSC was loaded by resistors to obtain active power $P = 3$ kW. The i_q^* was 0 A to achieve reactive power $Q = 0$ Var. In the examined algorithm with fixed virtual VVs the number of subdivisions of the sampling time T_s was 3.

As shown in Fig. 10(b), the best result is achieved for the new control method with floating virtual VVs. The FCS-MPC with fixed virtual VVs [see Fig. 10(a)] has larger current ripples, despite of analyzed 38 virtual VVs. The THDi factor of the grid current during steady state is compared in Table III.

The proposed FCS-MPC with floating virtual VVs was examined also during various grid voltage conditions [see Fig. 11]: test under unbalanced ($e_a = 75\%$ of the nominal value) and higher harmonics (THDu = 7.1% distorted by 5% of fifth and seventh harmonics) as well as single-phase voltage dip test ($e_a = 50$ % of the nominal value). In all the examined variants the grid current is sinusoidal and the algorithm tracks the reference current. Even during a single-phase voltage dip, the transient states are invisible [see Fig. 11(b)]. The results confirm that the proposed algorithm is highly resistant to disturbances in the grid voltage.

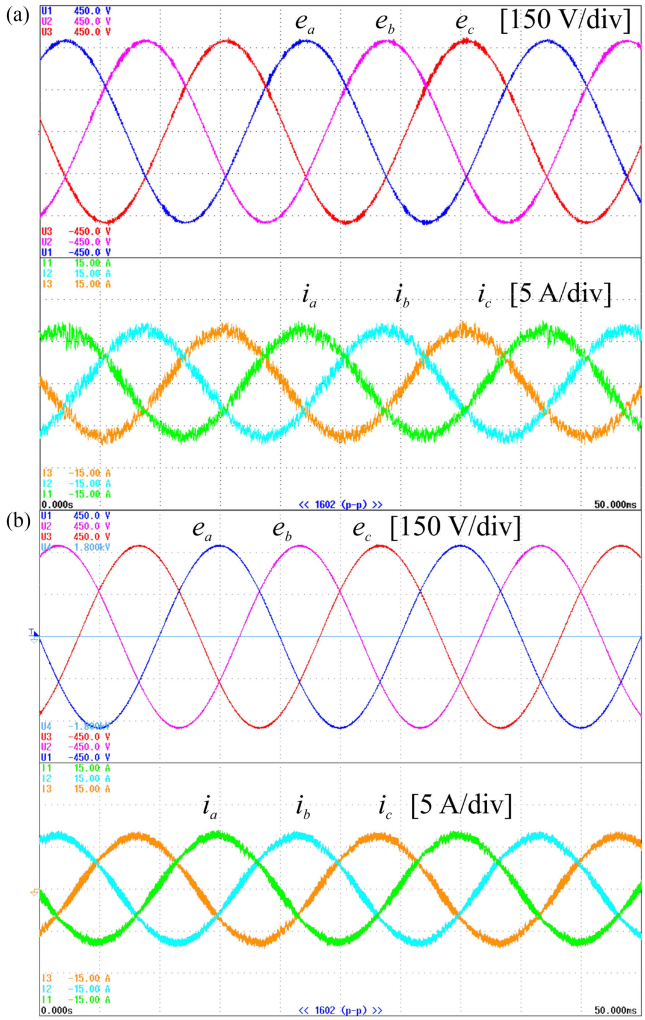

Fig. 10. Grid phase voltages and currents in a steady state for two control strategies: (a) FCS-MPC with fixed virtual VVs, (b) proposed FCS-MPC with floating virtual VVs.

Dynamic performances of the presented method are shown in Fig. 12. In order to eliminate the impact of the voltage-controller $U_{\rm dc}$ in the dc-link, tests were carried out in an open-loop system. The reference value step of the grid current $i_d^* = 6$ A→10 A→6 A (3 kW→5 kW→3 kW) was carried out while the reactive reference current remained constant $i_q^* = 0$ A. As one can notice the proposed method is characterized by high dynamic in the conditions of step changes of the references.

VIII. SUMMARY OF FCS-MPC WITH FLOATING VIRTUAL VVs

The presented FCS-MPC with floating virtual VVs can be characterized as follows in comparison to the method with fixed virtual VVs as following:

1) the reference voltage vector $\boldsymbol{u}_{dq}^*$ was introduced as one of analyzed by cost function VVs, that guarantees the lowest current ripples;
2) floating virtual VVs are independent to the number of sampling period subdivisions;

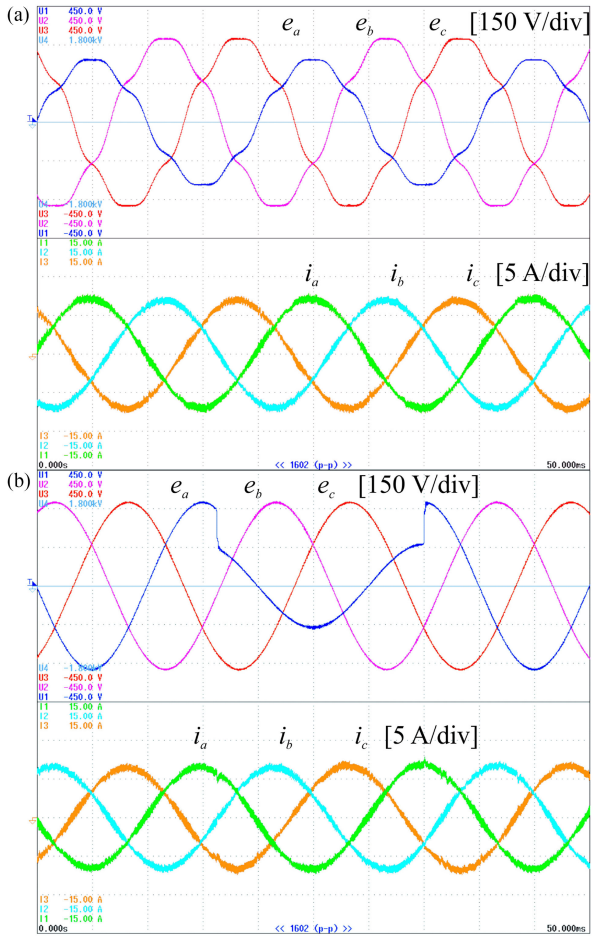

Fig. 11. Performances of the FCS-MPC with floating virtual VVs under various grid voltage conditions such as: (a) distorted and unbalanced grid voltage at the same time, (b) single phase grid voltage dip (the voltage e_a dropped to 50% of the nominal value).

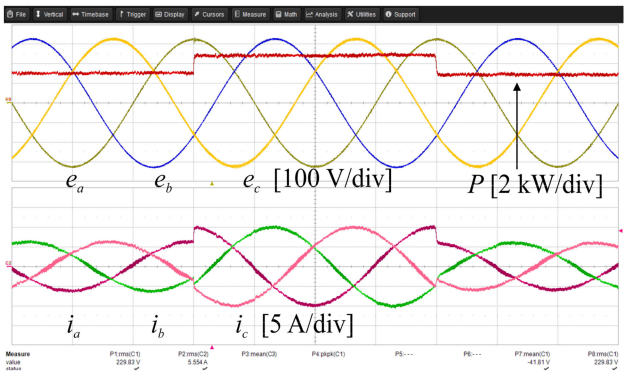

Fig. 12. Performances of the FCS-MPC with floating virtual VVs during transient states. The waveforms of the active power, grid phases voltages, and currents.

3) floating virtual VVs are much closer to the desirable actual voltage vector $\boldsymbol{u}_{1h}$, that allows us to minimize grid current ripples;
4) lower calculation burden;
5) not required use of preselection technique;
6) there is a continuous adjustment of floating virtual VVs to the optimal operating point.

IX. Conclusion

The FCS-MPC with floating virtual VVs has been proposed. The new control technique outperforms the compared methods in terms of lower THDi factor of the grid current and higher robustness to the filter inductance changes. Furthermore, it assures a constant switching frequency (solves one of the main disadvantages of conventional FCS-MPC). During simulation and experimental validations, the presented control method proved to be characterized by high dynamic response and robustness in the case of unbalanced and distorted grid voltage conditions as well as parameter variations.

References

[1] N. Muller, S. Kouro, M. Malinowski, C. A. Rojas, M. Jasinski, and G. Estay, "Medium-Voltage power converter interface for multigenerator marine energy conversion systems," *IEEE Trans. Ind. Electron.*, vol. 64, no. 2, pp. 1061–1070, Feb. 2017.
[2] T. Dragicevic, "Model predictive control of power converters for robust and fast operation of AC microgrids," *IEEE Trans. Power Electron.*, vol. 33, no. 7, pp. 6304–6317, Jul. 2018.
[3] J. Dannehl, C. Wessels, and F. W. Fuchs, "Limitations of voltage-oriented PI current control of grid-connected PWM rectifiers with LCL filters," *IEEE Trans. Ind. Electron.*, vol. 56, no. 2, pp. 380–388, Feb. 2009.
[4] Y. Zhang, J. Liu, H. Yang, and J. Gao, "Direct power control of pulsewidth modulated rectifiers without DC voltage oscillations under unbalanced grid conditions," *IEEE Trans. Ind. Electron.*, vol. 65, no. 10, pp. 7900–7910, Oct. D2018.
[5] K. Kulikowski and A. Sikorski, "New DPC look-up table methods for three-level AC/DC converter," *IEEE Trans. Ind. Electron.*, vol. 63, no. 12, pp. 7930–7938, Dec. 2016.
[6] Z. Song, Y. Tian, W. Chen, Z. Zou, and Z. Chen, "Predictive duty cycle control of three-phase active-front-end rectifiers," *IEEE Trans. Power Electron.*, vol. 31, no. 1, pp. 698–710, Jan. 2016.
[7] A. Timbus, M. Liserre, R. Teodorescu, P. Rodriguez, and F. Blaabjerg, "Evaluation of current controllers for distributed power generation systems," *IEEE Trans. Power Electron.*, vol. 24, no. 3, pp. 654–664, Mar. 2009.
[8] P. Cortes, M. P. Kazmierkowski, R. M. Kennel, D. E. Quevedo, and J. Rodriguez, "Predictive control in power electronics and drives," *IEEE Trans. Ind. Electron.*, vol. 55, no. 12, pp. 4312–4324, Dec. 2008.
[9] Y. Zhang, Y. Peng, and H. Yang, "Performance improvement of two-vectors-based model predictive control of PWM rectifier," *IEEE Trans. Power Electron.*, vol. 31, no. 8, pp. 6016–6030, Aug. 2016.
[10] M. Mehreganfar, M. H. Saeedinia, A. Davari, C. Garcia, and J. Rodriguez, "Sensorless predictive control of AFE rectifier with robust adaptive inductance estimation," *IEEE Trans. Ind. Inform.*, vol. 15, no. 6, pp. 3420–3431, Jun. 2018.
[11] P. Falkowski, K. Kulikowski, and R. Grodzki, "Predictive and look-up table control methods of a three-level AC-DC converter under distorted grid voltage," *Bull. Polish Acad. Sci. Tech. Sci.*, vol. 65, no. 5, pp. 609–618, 2017.
[12] H. Yang, Y. Zhang, J. Liang, J. Gao, P. D. Walker, and N. Zhang, "Sliding-Mode observer based voltage-sensorless model predictive power control of PWM rectifier under unbalanced grid conditions," *IEEE Trans. Ind. Electron.*, vol. 65, no. 7, pp. 5550–5560, Jul. 2018.
[13] S. Vazquez, J. Rodriguez, M. Rivera, L. G. Franquelo, and M. Norambuena, "Model predictive control for power converters and drives: Advances and trends," *IEEE Trans. Ind. Electron.*, vol. 64, no. 2, pp. 935–947, Feb. 2017.
[14] J. I. Leon, S. Kouro, L. G. Franquelo, J. Rodriguez, and B. Wu, "The essential role and the continuous evolution of modulation techniques for voltage-source inverters in the past, present, and future power electronics," *IEEE Trans. Ind. Electron.*, vol. 63, no. 5, pp. 2688–2701, May 2016.
[15] K. Antoniewicz, M. Jasinski, M. P. Kazmierkowski, and M. Malinowski, "Model predictive control for three-level four-leg flying capacitor converter operating as shunt active power filter," *IEEE Trans. Ind. Electron.*, vol. 63, no. 8, pp. 5255–5262, Aug. 2016.

[16] H. Gao, B. Wu, D. Xu, R. P. Aguilera, and P. Acuna, "Model predictive switching pattern control for current-source converters with space-vector-based selective harmonic elimination," *IEEE Trans. Power Electron.*, vol. 32, no. 8, pp. 6558–6569, Aug. 2017.
[17] A. Godlewska, R. Grodzki, P. Falkowski, M. Korzeniewski, K. Kulikowski, and A. Sikorski, "Advanced control methods of DC/AC and AC/DC power converters—look-up table and predictive algorithms," in *Advanced Control of Electrical Drives and Power Electronic Converters*, J. Kabziński, Ed. Cham, Switzerland: Springer, 2017, pp. 221–302.
[18] M. Norambuena, S. Kouro, S. Dieckerhoff, and J. Rodriguez, "Reduced multilevel converter: A novel multilevel converter with a reduced number of active switches," *IEEE Trans. Ind. Electron.*, vol. 65, no. 5, pp. 3636–3645, May 2018.
[19] W. Xiong *et al.*, "A cost-effective and low-complexity predictive control for matrix converters under unbalanced grid voltage conditions," *IEEE Access*, vol. 7, pp. 43895–43905, 2019.
[20] P. Karamanakos, T. Geyer, and S. Manias, "Direct model predictive current control strategy of DC-DC boost converters," *IEEE J. Emerg. Sel. Top. Power Electron.*, vol. 1, no. 4, pp. 337–346, Dec. 2013.
[21] A. Dekka, B. Wu, V. Yaramasu, and N. R. Zargari, "Integrated model predictive control with reduced switching frequency for modular multilevel converters," *IET Electr. Power Appl.*, vol. 11, no. 5, pp. 857–863, 2017.
[22] C. A. Rojas, M. Aguirre, S. Kouro, T. Geyer, and E. Gutierrez, "Leakage current mitigation in photovoltaic string inverter using predictive control with fixed average switching frequency," *IEEE Trans. Ind. Electron.*, vol. 64, no. 12, pp. 9344–9354, Dec. 2017.
[23] P. Kakosimos and H. Abu-Rub, "Predictive control of a grid-tied cascaded full-bridge NPC inverter for reducing high-frequency common-mode voltage components," *IEEE Trans. Ind. Inform.*, vol. 14, no. 6, pp. 2385–2394, Jun. 2018.
[24] A. A. Ahmed, B. K. Koh, and Y. Il Lee, "A comparison of finite control set and continuous control set model predictive control schemes for speed control of induction motors," *IEEE Trans. Ind. Inform.*, vol. 14, no. 4, pp. 1334–1346, Apr. 2018.
[25] T. Geyer, "Algebraic weighting factor selection for predictive torque and flux control," in *Proc. IEEE Energy Convers. Congr. Expo. ECCE*, Jan. 2017, pp. 357–364.
[26] M. Norambuena, J. Rodriguez, Z. Zhang, F. Wang, C. Garcia, and R. Kennel, "A very simple strategy for high-quality performance of AC machines using model predictive control," *IEEE Trans. Power Electron.*, vol. 34, no. 1, pp. 794–800, Jan. 2018.
[27] F. Wang, S. Member, H. Xie, Q. Chen, S. A. Davari, and S. Member, "Parallel predictive torque control for induction machines without weighting factors," *IEEE Trans. Power Electron.*, vol. 35, no. 2, pp. 1779–1788, Feb. 2020.
[28] X. Zhang and B. Hou, "Double vectors model predictive torque control without weighting factor based on voltage tracking error," *IEEE Trans. Power Electron.*, vol. 33, no. 3, pp. 2368–2380, Mar. 2018.
[29] R. O. Ramirez, J. R. Espinoza, F. Villarroel, E. Maurelia, and M. E. Reyes, "A novel hybrid finite control set model predictive control scheme with reduced switching," *IEEE Trans. Ind. Electron.*, vol. 61, no. 11, pp. 5912–5920, Nov. 2014.
[30] L. Tarisciotti, P. Zanchetta, A. Watson, P. Wheeler, J. C. Clare, and S. Bifaretti, "Multiobjective modulated model predictive control for a multilevel solid-state transformer," *IEEE Trans. Ind. Appl.*, vol. 51, no. 5, pp. 4051–4060, Sep.–Oct. 2015.
[31] F. Donoso, A. Mora, R. Cárdenas, A. Angulo, D. Sáez, and M. Rivera, "Finite-Set model-predictive control strategies for a 3L-NPC inverter operating with fixed switching frequency," *IEEE Trans. Ind. Electron.*, vol. 65, no. 5, pp. 3954–3965, May 2018.
[32] S. Vazquez *et al.*, "Model predictive control with constant switching frequency using a discrete space vector modulation with virtual state vectors," in *Proc. IEEE Int. Conf. Ind. Technol.*, Churchill, VIC, Australia, 2009, pp. 1–6.
[33] K. S. Alam, D. Xiao, M. Parvez Akter, D. Zhang, J. Fletcher, and M. F. Rahman, "Modified MPC with extended VVs for grid-connected rectifier," *IET Power Electron,* vol. 11, no. 12, pp. 1926–1936, Oct. 2018.
[34] K. S. Alam, M. P. Akter, D. Xiao, D. Zhang, and F. M. Rahman, "Asymptotically stable predictive control of a grid-connected converter based on discrete space vector modulation," *IEEE Trans. Ind. Inform.*, vol. 15, no. 5, pp. 2775–2785, May 2018.
[35] M. Abdelrahem, F. Hamadto, A. Garikapati, and R. Kennel, "Multiple-Vector direct model predictive control for grid-connected power converters with reduced calculation burden," in *Proc. IEEE Int. Symp. Predict. Control Electr. Drives Power Electron.*, Quanzhou, China, 2019, pp. 1–6.
[36] J. Lee, J. Lee, H. Moon, and K. Lee, "An improved finite-set model predictive control based on discrete space vector modulation methods for grid-connected three-level voltage source inverter," *IEEE J. Emerg. Sel. Top. Power Electron.*, vol. 6, no. 4, pp. 1744–1760, Dec. 2018.
[37] H. Moon, J. Lee, and K. Lee, "A robust deadbeat finite set model predictive current control based on discrete space vector modulation for a grid-connected voltage source inverter," *IEEE Trans. Energy Conv.*, vol. 33, no. 4, pp. 1719–1728, Dec. 2018.
[38] Y. Wang *et al.*, "Deadbeat model-predictive torque control with discrete space-vector modulation for PMSM drives," *IEEE Trans. Ind. Electron.*, vol. 64, no. 5, pp. 3537–3547, May 2017.
[39] P. Cortes, J. Rodriguez, C. Silva, and A. Flores, "Delay compensation in model predictive current control of a three-phase inverter," *IEEE Trans. Ind. Electron.*, vol. 59, no. 2, pp. 1323–1325, Feb. 2012.

Piotr Falkowski received the M.Sc. and Ph.D. degrees in electrical engineering from Bialystok University of Technology, Bialystok, Poland, in 2012 and 2017, respectively.

His research interests include the areas of power electronics, model predictive control of ac/dc/ac back-to-back converters and drives.

Andrzej Sikorski received the M.Sc. degree from Bialystok University of Technology, Białystok, Poland, in 1980, the Ph.D. degree from Warsaw University of Technology, Warsaw, Poland, in 1989, and the D.Sc. degree from Poznan University of Technology, Poznań, Poland, in 2000, all in electrical engineering.

He has authored and coauthored more than 100 papers in technical journals and conference proceedings in 2011. He was bestowed professorship in technical sciences by the President of the Republic of Poland. His research interests include the areas of electric drives, power electronics, particularly ac/dc/ac back-to-back converters.

Mariusz Malinowski (Fellow, IEEE) received the Ph.D. and D.Sc. degrees in electrical engineering from the Institute of Control and Industrial Electronics, Warsaw University of Technology (WUT), Warsaw, Poland, in 2001 and 2012, respectively.

He is currently with the Institute of Control and Industrial Electronics, WUT. He has coauthored more than 150 technical papers and seven books. His current research interests include the control and the modulation of grid-side converters, multilevel converters, smart grids, and power-generation systems based on renewable energies.

Prof. Malinowski was a recipient of the IEEE IES David Irwin Early Career Award, IEEE IES Bimal Bose Energy Systems Award, Polish Prime Minister Award and the Polish Ministry of Science and High Education Award.